Potential of Radiotelescopes for Atmospheric Line Observations: I. Observation Principles and Transmission Curves for Selected Sites

Nicola Schneider [a,*], Joachim Urban [b], Philippe Baron [c]

[a] *IRFU/SAp CEA/DSM, Laboratoire AIM CNRS - Université Paris Diderot, F-91191 Gif-sur-Yvette, France*
[b] *Chalmers University of Technology, Department of Radio and Space Science, 412 96 Göteborg, Sweden*
[c] *National Institute of Information and Communication Technology, Koganei, Tokyo, Japan*

Abstract

Existing and planned radiotelescopes working in the millimetre (mm) and sub-millimetre wavelengths range provide the possibility to be used for atmospheric line observations. To scrutinize this potential, we outline the differences and similarities in technical equipment and observing techniques between ground-based aeronomy mm-wave radiometers and radiotelescopes. Comprehensive tables summarizing the technical characteristics of existing and future (sub)-mm radiotelescopes are given. The advantages and disadvantages using radiotelescopes for atmospheric line observations are discussed. In view of the importance of exploring the sub-mm and far-infrared wavelengths range for astronomical observations and atmospheric sciences, we present model calculations of the atmospheric transmission for selected telescope sites (DOME-C/Antarctica, ALMA/Chajnantor, JCMT and CSO on Mauna Kea/Hawaii, KOSMA/Swiss Alpes) for frequencies between 0 and 2000 GHz (150 μm) and typical atmospheric conditions using the forward model MOLIERE (version 5). For the DOME-C site, the transmission over a larger range of up to 10 THz (30 μm) is calculated in order to demonstrate the quality of an earth-bound site for mid-IR observations. All results are available on a dedicated webpage.

Key words: Radiotelescopes and instrumentation, Atmospheric transmission
PACS: 92.60.H, 93.30.Ca, 93.30.Ge, 93.30.Hf, 93.30.Jg, 95.45.+i, 95.55.-n, 95.55.Jz, 95.75.-z, 95.75.Rs, 95.85.Bh, 95.85.Fm, 95.85.Gn,

1. Introduction

1.1. *Atmospheric line observations with radiotelescopes*

The millimetre and sub-millimetre wavelengths range contains a large number of atmospheric emission lines of molecular transitions (rotational, rotation-vibration, hyperfine structure lines), including important atmospheric species such as H_2O, O_3, O_2, N_2O, HCl, ClO, OH, CO, among many others. Atmospheric scientists observe these molecules in different geometries (limb-, nadir-, and zenith-sounding) either with ground-based mm-wave radiometers in the frequency range of 20 to 300 GHz (15 to 1 mm) or with airborne and space-borne sensors (up to ∼2.5 THz or 110 μm), less affected by the absorption of water vapor in the Earth's troposphere. While the references for observations in the mm-wavelengths range are numerous, there are significantly fewer observation systems at high frequencies. Examples for satellite instruments are SMR (Sub-Millimetre Radiometer) on

* Corresponding author. Tel.: +33 169 08 2266; fax: +33 169 08 6577
Email addresses: nschneid@cea.fr (Nicola Schneider), joaurb@chalmers.se (Joachim Urban), baron@nict.go.jp (Philippe Baron).

Odin [Frisk et al., 2003], launched in 2001, working in the frequency band 486–580 GHz and the Microwave Limb Sounder (MLS) on Aura, operating several radiometers around 180, 230, 625–660 GHz, and at 2.5 THz since 2004 [Waters et al., 2006]. The launch for JEM/SMILES (Japanese superconducting submillimeter-wave limb-emission sounder) with a 640 GHz SIS radiometer is planned for late 2009 [Kasai et al., 2006].

Ground-based microwave radiotelescopes (RTs from now on) are normally devoted to perform radio-astronomical observations in the (sub)-mm region which is the typical emitting wavelength range for various transitions of molecules. More than 140 molecules have already been detected in space (with CO as the most abundant one after H_2) and the list is continuously growing. Planned facilities at extremely dry sites, such as DOME-C in Antarctica or CCAT (Cornell-Caltech Atacama Telescope) in the Andes, would enable to access even the THz range and thus observations of interesting atomic and ionic lines like ionized nitrogen, [NII], at 1.46 THz, and molecular transitions like high-J CO, HCN, and HCO^+ lines and light hydrides (NH^+, NH_2 etc.) would become possible. These tracers are used to study the physics of UV illuminated regions or very dense star forming regions.

The technical equipment and observing procedures are originally designed for astronomical observations that normally cancel out the atmospheric contribution. In addition, RTs always work in uplooking geometry. However, using special observing methods, RTs already have been used in the past to make sporadic measurements of the line emission of atmospheric species (e.g. H_2O, Barret and Chung [1962]; Groom [1965]; Bevilaqua et al. [1983]; HO_2, Sandor and Clancy [1998]; O_3, Caton et al. [1968], Connor et al. [1987]; ClO, Parrish et al. [1981], Solomon et al. [1984]; CO, Waters et al. [1976]), and to perform long-term monitoring projects (e.g. CO, Boes [1994]). O_2-Zeeman splitting was observed by Pardo et al. [1995]. The typical altitude range covered by these observations is 10–80 km with an altitude resolution ranging from 5–20 km. Going down much lower in altitude is not always useful because (i) the molecular line is very broad and spectrally not resolved due to the limited bandwidth of the receiver, and (ii) absorption (= emission) is dominated by water vapor and dry air and thus a line can not be separated from the water vapor and dry air continuum

The motivations for observing atmospheric lines are mannifold. Many mm-wave heterodyne instruments belong to the "Network for Atmospheric Composition Change" (NDACC, http://www.ndsc.ncep.noaa.gov). These and other radiometers focus on the short and long term abundance variations of stratospheric ozone [e.g. Sinnhuber et al., 1998; Calisesi et al., 2001; Klein et al., 2002; Schneider et al., 2003; Raffalski et al., 2005; Steinbrecht et al., 2006] as well as strato-mesospheric water vapor [e.g. Seele and Hartogh, 1999; Nedoluha et al., 2003]. A large number of molecules of prime interest for middle atmospheric sciences, often having only very low abundances, can be observed and studied using this remote technique. Besides, (mainly campaign-based) observations of key species related to polar ozone depletion such as ClO and HNO_3 [Shindell and de Zafra, 1996; de Zafra and Smyshlyaev, 2001; Muscari et al., 2002], and longer-lived species such as N_2O and CO have been succesfully measured. They are particularly useful as tracers of middle atmospheric transport [e.g. Crewell et al., 1995; de Zafra and Muscari, 2004; Forkman et al., 2005]. Another example is the observation of the atmospheric HCN molecule that has been detected at three different radio-astronomical observatories, i.e. the *Cologne Observatory for Sub-mm Astronomy* (KOSMA, Gornergrat, Switzerland), the *James Clark Maxwell Telescope* (JCMT, Mauna Kea, Hawaii), and the *Caltech Submm Observatory* (CSO, Mauna Kea, Hawaii) [e.g. Despois et al., 2000; Lautié, 2003]. These measurements will be further discussed in another paper [Lautié et al. 2009 in prep., Paper-II]. A dedicated instrument routinely used on an astronomical telescope (the CSO) for atmospheric studies is a Fourier Transform Spectrometer [Pardo et al., 2004].

RTs are also powerful tools to study the chemistry in the upper stratosphere and mesosphere [Sandor and Clancy, 1998]. They can record the diurnal variations of atmospheric trace gases and, hence, complete observations from sun-synchronous orbiters, which are at fixed local times. Furthermore, observations with RTs can provide a database of rarely observed molecules to validate satellite observations and can be used for observations of the atmosphere of other planets in the solar system. Finally, RTs can also be used to derive mesospheric wind vectors from the Doppler-shift of observed lines [Burrows et al., 2007].

Due to the increase of the tropospheric back-

ground absorption (dominated by water vapor and dry air continuum) with frequency throughout the mm- and sub-mm wavelengths range, spectral windows with sufficiently low optical thicknesses for ground-based observations of middle atmospheric target species can mainly be found at frequencies smaller than ∼300 GHz. Since, at the same time, the line intensities of most minor species increase with frequency in the sub-mm range, highest possible frequency windows are of interest and measurements shall preferably be performed at extremely dry sites, similar to radio-astronomical observations. However, the maximum upper limit for obtaining a profile and not only a column, i.e. the altitude of the transition from pressure to Doppler broadened lines, decreases with rising frequency. It is typically 90 km at 100 GHz and 70 km at 2 THz.

In order to efficiently use RTs for atmospheric line observations, it is mandatory to have an overview of available front- and back-ends of existing and planned RTs and to fully understand the employed observing techniques. For this reason we present in this paper a short review of the basic principles how radio-observations are performed and summarize in detail the main properties of the instruments. Comprehensive tables including all astronomical (sub)-mm facilities are given.

1.2. *Transmission curves*

For both, astronomical and aeronomy observations in the sub-mm/far-infrared (FIR) range, it is of prime importance to assess the quality of the atmosphere in terms of transparency. Only extremely dry sites allow to access this spectral range. We therefore used the forward model MOLIERE-5 [Urban et al., 2004a] to predict the atmospheric transmission for sites of interest for sub-mm/FIR astronomy. In this paper, we show the results for frequencies between 0 and 2000 GHz for the sites of Chajnantor/Chile, DOME-C/Antarctica, Mauna Kea/Hawaii, and KOSMA/Swiss Alps. A more comprehensive list of observatories covering different wavelengths and various regimes of atmospheric conditions is made available on http://transmissioncurves.free.fr. In Paper-III of this series (Schneider et al., 2009, in preparation) we compare the results obtained with MOLIERE-5 to other atmospheric models used in radioastronomy, i.e. ATM (Atmospheric Transmission at Microwaves, Pardo et al. [2001]), ATRAN (Atmospheric TRANsmission, Lord [1992]), and AM (Atmospheric Model, Paine [2004]).

2. Radiotelescopes vs. mm-wave radiometers

In this section, we summarize the principal similarities and differences between mm-wave radiotelescopes and aeronomy radiometers. An overview of the sites is given in Table 1 (as of summer 2009 see individual websites given in column 6 for more recent information), and the main instrumental characteristics are summarized in Table 2.

2.1. *Technical equipment*

2.1.1. *Optics*

Millimeter-wave RTs are movable, single, parabolic dishes with 1 to currently 45 m diameter. The emission is received in the main dish and reflected on the subreflector. The *Half Power Beam Width* (HPBW) depends on the telescope diameter d and the observing frequency ν (HPBW [′] $\sim$ 1260/(d [m] $\times$ ν [GHz]) and varies typically between 0.1′ (300 GHz @ 30m) and 11′ (100 GHz @ 1 m).

In contrast, aeronomy heterodyne receivers are normally non-steerable instruments with a focusing mirror or horn antenna as entrance aperture, leading to large beam sizes of typically a few degrees. The size of the beam as well as a possible error-beam pickup is normally unimportant for atmospheric observations.

2.1.2. *Front-end*

Both types of instruments use the superheterodyne principle [Kraus, 1986] to convert the high frequency signal f_S via a mixer into a low-frequency intermediate signal f_{IF}. Due to the mixing process with a signal from a local oscillator f_{LO}, two major frequencies are produced: f_{LO}–f_S and f_{LO}+f_S. Heterodyne receivers can work in double- (DSB) or single-sideband mode (SSB), depending on whether the detector receives both side bands or whether one is suppressed. In the latter case, one of the bands f_{LO}–f_S or f_S–f_{LO} can be choosen. Aeronomy line observations are normally performed in SSB mode in order to prevent confusion of pressure-broadenend lines from both sidebands.

Critical parameters for the detection of a signal T_{sig} [K] are the frequency resolution $\Delta\nu$ [Hz], system noise temperature T_{sys} [K] and integration time t_{int} [s]. We define the system noise temperature as

the sum of the receiver noise temperature and the signal brightness temperature: $T_{sys} = T_{rec} + T_{sig}$ [K]. The rms noise is $\Delta T_{rms} = T_{sys}/\sqrt{(\Delta\nu\, t_{int})}$. However, the radiometer formula is only correct as long as the receiver noise is thermal in nature. The time when the Allan variance [Allan, 1972] has a minimum ("Allan minimum time"), is the maximum integration time up to which the noise decreases with integration time. The integration time should therefore not be longer than this Allan minimum time. It is typically in the range of a few seconds up to several tens of seconds.

The receiver temperature depends critically on the mixer and first amplifier in the chain. *Schottky-diode* mixers use the non-linear current-voltage characteristic of metal/semi-conductor diodes for the mixing process and reach typically noise temperatures of a few hundreds to one thousand Kelvin (double sideband mode, 100 to 400 GHz). SIS (*Semiconductor-Insulator-Semiconductor*) receivers on the other hand, reach DSB noise temperatures as low as around 80 to 200 K in the same frequency range.

RTs nowadays employ SIS receivers up to 1 Terahertz (THz) which are cooled by a reservoir of liquid helium or a closed-cycle system. The same is true for stationary aeronomy radiometers though Schottky systems are still employed due to their easy handling and robustness. This is an important criteria for automatic operation over long time periods in remote locations. Many of these receivers are tuned to a fixed frequency in order to monitor a particular spectral line (e.g O_3, H_2O). Recent developments to reach higher frequencies – both, in aeronomy and astronomy – employ *Hot Electron Bolometers* (HEB) that operate as heterodyne mixer elements for down conversion of the observed signal into an intermediate frequency signal. For example, the HEB instrument CONDOR (CO N^+ Deuterium Observations Receiver, Wiedner et al. [2006],Wieching [2007]) working between 1.3 and 1.5 THz, was successfully installed at the APEX radiotelescope in Chile.

2.1.3. *Back-end*

Spectroscopy of (sub)mm-wave molecular and atomic lines requires a real-time spectrometer in combination with the heterodyne receiver. Different types of such spectrometers are available, namely 'filterbanks', 'chirp-transform spectrometers (CTS)', 'auto-correlators' (AC), 'acousto-optical spectrometers (AOS)', and 'FFTS' (Fast Fourier Transform Spectrometer). While CTS offer only relatively small bandwidths, all other instruments have been built with bandwidths of the order of 1–4 GHz which is important for the detection of pressure-broadened atmospheric lines in order to cover the contributions to the spectrum originating from low altitudes (typically a few to 20 km). An equidistant resolution over the whole bandwidth is usually required. Upper atmosphere sounding requires a frequency resolution of the order of 0.1–1 MHz. Bandwidth and spectral resolution of a filterbank spectrometer are in principle flexible design parameters, however with increasing bandwidth and high spectral resolution this type of instrument is getting voluminous and unpractical. Thus, AOS, AC, and FFTS are often the preferred choice for both, aeronomy and astronomy, measurement systems.

2.2. *Observing Methods*

2.2.1. *Radiotelescopes*

The definition for observing with RTs is that a *signal* position refers to the emitting astronomical source and a *reference* position to an emission free position away from the astronomical source. In the following, we give an overview of all observing methods employed for observations using RTs. Figure 1 shows measurements of mesospheric CO, taken at the KOSMA 3m telescope, to illustrate the observing methods suitable for atmospheric line measurements.

Position-switching (PS)

This is the most simple observing mode for RTs. The telescope observes alternately the signal and the reference position, the latter being subtracted from the signal. This procedure eliminates most instrumental and atmospheric effects, accordingly it is not suitable for telluric lines. The integration time may be adapted to the total system stability time determined by the Allan variance method [Allan, 1972]. Standing waves in the optical path appear as frequency dependent baseline ripples in the spectrum. Moving the sub-reflector between the signal- and reference phases by 1/4 of the observing wavelength can help to compensate for this effect. We succesfully employed this correction-method for our frequency-switching atmospheric HCN observations at the KOSMA radiotelescope (Paper II).

Beam Switching (BS)
For this observing mode, the secondary mirror is tipped by a small angle ('chopped') at a choosen frequency and amplitude ('throw'). The detected signal is the difference between the sky and reference signals. The advantage of this method is that switching can be performed much faster than with the PS method but the switch throw is normally limited in distance to the source (up to a few 10′). This method also naturally cancels out atmospheric lines.

Frequency Switching (FS)
In this case, the frequency of the local oscillator is switched between two values of the LO frequency (f and f+δf), separated by typically a few to a few tens of megahertz, whilst observing only in the signal path. Both spectra (S(f) and S(f+δf)) are then subtracted so that in the final spectrum S1 = S(f+δf) – S(f), a positive and a negative line appear (see Fig. 1a). A modification of simple FS is the 'Double frequency switching' mode in which the LO is also switched in the opposite direction (f–δf), leading to an additional spectrum S2 = S(f) – S(f–δf). The final spectrum can then be computed as S = 0.5 (S1 – S2) = S(f) – 0.5×S(f–δf) – 0.5×S(f+δf).

If the LO system (normally stabilized by a phase locked loop) is not stable enough to support fast switching, FS can be mimiced by switching the frequency every signal phase (typically 20–40 s). All FS procedures enable to observe atmospheric lines directly. However, if a frequency range with a high density of spectral lines is observed, crowding and overlapping of spectral features can be a problem, in particular if working in DSB mode. Broad lines such as those from ozone in the lower stratosphere are very critical whereas narrow lines like mesospheric CO are less critical. If the frequency throw is too small, the line wings of a pressure-broadened line are cut off, restricting the exploitable altitude range.

Load Switching (LS)
If the reference position is not taken on the sky, as for total power, but on the cold load of the receiver, formally a spectrum can be calculated by subtracting the load spectrum from the signal spectrum (see Fig. 1b). Atmospheric lines are generally observable with this method but the continuum offset between cold load (liquid nitrogen at 77 K) and sky is large and standing waves are typical so that this method is not appropriate for detecting weak lines.

Absorption measurements (AM)
Absorption measurements against Sun, Moon or mountains are performed in a similar way as for load switching by replacing the cold load with the astrophysical object or mountain (see Fig. 1c and 1d). However, the calibration of these spectra is often difficult due to large differences in the continuum level and due to the fact that neither mountains nor planets, moon, or sun are perfectly emitting as a blackbody.

2.2.2. *Aeronomy Receivers*

Total Power
Strong atmospheric lines can be observed using a total power method, i.e. the sky measurement is performed at a fixed elevation angle and the received signal is calibrated in frequent intervals with measurements of a hot and cold calibration source. As explained above, baseline ripples due to standing waves in the optical paths may be suppressed by using a phase-wobbler which frequently changes the optical path lengths (e.g. by 1/4 of the observing wavelength).

Load switching and Frequency Switching
These procedures (described in Sec. 2.2.1) may also be used for aeronomy observations. See for example Ricaud et al. [1991] for a detailed description and application of the frequency-switching technique for ozone observations as well as Lobsiger et al. [1984] for load switching ozone measurements.

Balanced Beam Switching (BBS)
This commonly employed differential observing method was initially developed by Parrish et al. [1988]. It uses an atmospheric measurement at low elevation (typically between 10° and 20°) resulting in a large emission path length along the line-of-sight, providing a strong signal, and a reference measurement (R) at higher elevation (typically >50°) with a much weaker emission strengths. In order to compensate for the offset in the received power between the two views, an absorber (such as a plexiglass plate) is put in the reference path. Fine balancing of the power levels in signal and reference path is achieved by varying the elevation angle of the signal view. The difference S–R then contains the differential signal emission in which –to first order– instrumental effects such as receiver non-linearities and standing waves are removed. This technique is

commonly employed by ground-based radiometers within the framework of the NDACC.

Balanced Load Switching (BLS)
An alternative to the beam switching technique is the *Balanced Load Switching (BLS)* method, where the reference watches the cold load instead of the atmosphere and the balancing is achieved by mixing the cold signal with an absorber at ambient temperature using a turnable wire grid [e.g. Raffalski et al., 2005]. This procedure is similar to the 'Dicke-switching' method used in radioastronomy.

2.3. *Correction of tropospheric absorption*

Outside the line centres, the atmospheric transmission relevant to an observer at the ground is determined by the tropospheric absorption whilst strato-mesospheric lines and continua have typically only a negligible contribution. The most important factor for the tropospheric transmission is the (frequency dependent) tropospheric water vapor profile. Atmospheric emission (and absorption) is a function of temperature. Spectral line broadening as well as collision induced non-resonant continuum absorption are also functions of pressure.

By using a mechanical or software simulated 'chopper-wheel' calibration or a 'sky dip' measurement, the troposheric opacity τ is calculated and the detected emission in terms of calibrated antenna temperature T'_A [K] can be corrected as

$$T_A = T'_A \exp(-\tau\, A)\ [K]. \qquad (1)$$

$A \approx 1/\sin(elevation)$ is the geometrical air mass factor. The 'sky dip' method consists of measuring either distinct points or continuously the atmospheric emission from high to low elevations and derive the opacity by an exponential fit to equation 1. The 'chopper wheel' calibration [Penzias and Burrus, 1973] defines the calibration signal to be the difference between an absorber at ambient temperature and the sky. Finally, the calibrated antenna temperature has to be corrected for the telescopes forward- and main beam efficiency to derive main beam brightness temperatures [see e.g. Kraus, 1986].

2.4. *Requirements for astronomical and atmospheric observations*

Astronomical observations with single dish RTs typically require an absolute calibration accuracy of lower than 10%, an equidistant, good frequency resolution, and a good pointing accuracy (better than 20% of the beamsize). The required beamsize depends on the astronomical project, i.e. large beamsizes for efficiently mapping large areas on the sky, small beamsizes for extragalactic and detailed Galactic studies. For atmospheric line observations, the calibration should ideally be better than 1%, including sideband ratio calibration and tropospheric correction. Pointing and beamsize are less important but the requirements for long-term stability and good baselines are high. Both, high-resolution frequency observations (e.g. narrow lines in the mesosphere) and broadband observations (broad lines in the troposphere and lower stratosphere) are important.

2.5. *Characteristics of Radiotelescopes*

Table 1 lists all radiotelescopes operating in the mm- and sub-mm wavelengths range with an antenna radius between ∼1 m and 45 m which can potentially perform atmospheric observations. Four of them are located in Europe, five in the US (two of those in Hawaii), three in South America (Chile), three in Asia, and one in Australia. Eight telescopes are situated at high altitude sites (>3000 m). Not listed are mm- and sub-mm interferometers though it can be of interest to use these explored sites to install aeronomy radiometers. For example, a radiometer monitoring ClO [Ricaud et al., 2004] was placed on the Plateau de Bure in the French Alps, hosting an interferometer with 6 mm-antennas of 15 m size (http://iram.fr). Other locations are the *Submillimeter Array* (http://sma-www.harvard.edu/) in Hawaii/USA, the *Combined Array for Research in Mm-wave Astronomy* (CARMA, http://www.mmarray.org) located in California/USA, the *Australia Telescope Compact Array* (ATCA, http://narrabri.atnf.csiro.au), and the Nobeyama Millimetre Array (NMA, http://www.nro.nao.ac.jp). The Atacama Large Millimetre Array (ALMA) with at least 50 dishes of 12m diameter each is currently being constructed on the plateau of Chanjantor and is expected to be

operational with some antennas starting from 2012. A 50m single dish sub-mm-RT (the Large Millimetre Telescope, LMT, http://www.lmtgtm.org) is set up in Mexico and foreseen to receive first light in 2009. Other sites under investigation for sub-mm RT are located in Chile (the Cornell-Caltech Atacama Telescope CCAT, http://www.submm.org) and Antarctica (DOME-C at the Concordia Station, DOME-A at 80°S on the Antarctican Plateau at an altitude of 4093m, and DOME-F at 77°S at an altitude of 3810m).

The technical specifications of the telescopes listed in Table 1 are given in Table 2. We do not include bolometers in this list since we focus on spectroscopy. However, using bolometers can be interesting for the study of atmospheric emissivity changes due to pwv or broad planetary absorption lines. For most of the telescopes, different receivers in various tuning ranges are available. Please note that all back-ends can usually be attached to all front-ends and are thus given in just one line of the table.

Nearly all radiotelescopes use SIS mixers that provide low receiver noise temperatures and work in DSB mode, in which emission from the upper and lower sidebands are overlaid and indiscriminately detected. The receivers have large tuning ranges although for some RTs, certain frequency windows are intentionally excluded (e.g. the 280–320 GHz or 380–420 GHz range) since the atmosphere is opaque at these frequencies due to strong H_2O and O_2 line absorption. As back-ends, acousto-optical spectrometers, filterbanks, and recently Fast Fourier Transform Spectrometers are widely distributed and offer a wide range of bandwidths and spectral resolutions. The receiver bandwidth is typically around 1 GHz.

3. Using radiotelescopes for atmospheric line observations

The HCN observations presented in Paper-II, performed using three well-known sub-mm radiotelescopes, together with a long tradition to use RTs for sporadic measurements of atmospheric lines raise the question how useful RTs are for such measurements. In particular with respect to new antennas (ALMA, LMT) and envisaged projects (DOME-A/C, CCAT) it is of great interest to explore the possible use of these telescopes for observing telluric lines. Accompanying the exploitation of these very good observing sites, the technical development of front- and back-ends opens now also the possibility to observe up to a frequency of 1.5 THz using broad band (bandwidth > 2 GHz) receivers and spectrometers. This would enable to observe a number of interesting molecular and possibly atomic species at high-frequencies covering the stratosphere and mesosphere. Due to the high sensitivity and angular resolution, it is now also feasible to investigate the atmosphere of other planets (e.g. detection of CO and other molecules in the Martian atmosphere, see Encrenaz et al. [2004] for a summary).

In the following, we summarize advantages and disadvantages of using RTs for atmospheric line observations:

Advantages

- RTs are installed on explored sites that offer well-developed logistics and simple access (exceptions are DOME-A, C and F in Antarctica). The geographical coverage is large though only a few instruments exist at high latitudes. The use of RTs is normally open to the aeronomy community and observing time can be granted via proposals or guaranteed time.
- Some telescopes have spare time that is not used for astronomical observations and could be allocated for aeronomy measurements. Examples are the JCMT during daytime or Mopra and KOSMA during the summer period.
- RTs are flexible measurement systems providing front-ends and back-ends suitable for a wide range of applications, ranging from observations of strong narrow lines that require a high spectral resolution to measurements of weak broad features (rare and complex molecules in the atmosphere, observations of external galaxies and the Galactic center). Of particular interest for aeronomy is the detection of weak and pressure-broadened lines which is feasible by the provided technical equipment. Nearly all RT receivers are of SIS type, providing very low noise temperatures (typically <100 K @ 200 GHz). New instruments using HEBs (Hot Electron Bolometer) extend the accessible frequency range up to ∼1–2 THz.
- RTs have implemented robust and well tested methods for precise calibration to obtain correct main beam brightness temperatures (see Sec. 2.2.1). The calibration error, however, can be of the order of 5–10%, depending on site and weather conditions. Standard procedures to determine the tropospheric opacity are also provided

(see Sec. 2.3). As an additional feature, astronomical sources of well-known emission strength can be used in two ways for improving the calibration (for example the sideband-ratio): (i) the astronomical object is observed *before* and *after* the aeronomical observation or (ii) the astronomical object is all the time visible in the spectrum. In the latter case, blending of lines has to be avoided.
- RTs offer possibilities to overcome baseline problems due to standing waves and reflections by moving the subreflector by $\lambda/4$ or by random moving.
- RTs are steerable instruments and can thus be used for skydips and/or scanning the atmosphere.
- Standard software tools are usually available for RT operation and calibration.

Disadvantages
- Since the instruments are not movable, the geographical location of RTs is restricted to certain geographical areas on the globe.
- Observing time – in particular for the sub-mm telescopes and for a sophisticated instrument like ALMA – is very valuable and sometimes difficult to obtain. Long-term monitoring projects are thus hard to realize unless spare time (e.g. daytime at JCMT, see above) is efficiently used. This, however, may impose a bias on the observations depending on the scientific application. For example, it may be difficult to observe diurnal and seasonal variations of some molecules as well as to analyse their long-term variability.
- RTs are not concepted for atmospheric measurements so that special observing techniques (e.g. subreflector movement for the reduction of standing waves) are often not implemented in the normal procedures. However, astronomical observations may benefit from optimisations and standard implementation of these techniques as well.
- A calibration uncertainty of up to 10% can be too high for certain aeronomical applications that demand a high precision. Pure detection projects or monitoring of strong lines (for example mesospheric CO) are not problematic.

Considering the pro and contra arguments for the use of radiotelescopes for atmospheric line observations, we come to the conclusion that RTs offer indeed a very good opportunity for certain applications in aeronomy. In particular exploratory observations of 'exotic' and thus probably weak lines or high-frequency transitions of standard molecules can easily be performed with RTs before a dedicated aeronomy receiver is built and installed for long-term monitoring of trends and variability. It should, however, be considered that the atmospheric abundance of some molecules of interest for aeronomy is high enough only at high latitudes where currently no (sub)-mm telescope is installed. Long-term monitoring projects of standard molecules with strong lines – like e.g. the observation of strato-mesospheric CO – are easy to do with standard RT observing modes and have in fact already been realized [e.g. Boes, 1994, 7-year time series of atmospheric CO using KOSMA].

4. Prediction of the Earth's atmospheric transmission

4.1. *Introduction*

The simulation of the atmospheric transmission is essential for all astronomy and middle atmospheric applications. In *astronomy*, the knowledge of atmospheric transmission at a given frequency is mandatory to asses the quality of an existing or future observatory site. It is also essential for the calibration since it is required to calculate the system noise temperature in case the opacity is not independently determined. *Remote observations* of the Earth's middle atmosphere require to model accurately the observed emission spectra. 'Forward models' are used to describe the radiative transfer, spectroscopy, and instrument characteristics and to compute weighting functions with respect to the searched atmospheric quantities. A versatile forward and inversion model for the (sub)-mm wavelengths range used in many aeronomy applications is the MOLIERE-5 code (*Microwave Observation LIne Estimation and REtrieval*). See Schneider et al. [2003]; Urban et al. [2004a]; Kasai et al. [2006] for its use for the analysis of ground-based and airborne microwave observations, and Urban et al. [2005b, 2007a] for applications with respect to space-borne missions. MOLIERE-5 has also been used for prediction/feasibility studies of future satellite projects for the exploration of the Earth and Mars atmospheres [Urban et al., 2000a, 2005a].

There are other atmospheric models that have been used to date (see Pardo et al. [2001] for a short summary). A discussion of these models and a comparison with MOLIERE-5 is the subject of Paper-III (Schneider et al. 2009, in prep.). Here we focus

on a short description of MOLIERE-5 and present the results of the modeled atmospheric transmission in the sub-mm/FIR range for different observatory sites.

4.2. *The forward model MOLIERE-5*

A detailed mathematical description of the MOLIERE-5 forward and inversion model and the underlying principles is provided by Urban et al. [2004a]. Designed for a variety of applications, the model comprises modules for spectroscopy, radiative transfer, and instrument characteristics. Important features of the absorption coefficient module are the line-by-line calculation as well as the implemented H_2O, O_2, N_2, and CO_2 continuum models [Borysow and Frommhold, 1986; Clough et al., 1989; Liebe et al., 1993; Rosenkranz, 1993; Pardo et al., 2001]. Note that MOLIERE-5 is a 'clear-sky' model that simulates atmospheric gas-phase emission and absorption. It does not include the radiative effect of cloud droplets or ice (see, e.g., Prigent et al. [2006] for a discussion of this effect).

The radiative transfer module allows for calculations in different geometries such as limb and nadir sounding from orbiting platforms as well as up-looking observations of ground-based or airborne sensors. A spherically stratified (1-D) emitting and absorbing (non-scattering) atmosphere in local thermodynamical equilibrium is assumed, i.e. the source function is given by Planck's function. The geometrical radiation path is corrected for the effect of refraction. Weighting functions, required for inversions, are calculated by differentiating the radiative transfer equation analytically after discretisation. The radiative transfer model is supplemented by a sensitivity module for estimating the contribution to the spectrum of each catalogue line at its centre frequency, enabling the model to effectively filter large spectral data bases for relevant spectral lines.

The spectroscopic parameters used in MOLIERE-5 are obtained from the VERDANDI catalog [Eriksson, 1999] that contains the JPL [Pickett et al., 1998] and HITRAN [Rothman et al., 1998] line parameters up to 10 THz. The catalog is updated regularly and available at http://www.chalmers.se/rss/. We included all spectral lines in this catalog of molecules with a contribution of 0.1 K brightness temperature to the spectrum up to 10 THz.

Several independent modules permit accurate simulation of instrument characteristics such as the antenna field-of-view, the sideband response of a heterodyne receiver, as well as the spectrometer bandwidth and resolution. Frequency switched observations may also be modelled. These features, however, were not used for the forward-calculations presented here but are required to model real observations. This particular feature makes MOLIERE-5 a very useful tool for aeronomy and astronomy applications and makes it different from other atmospheric models where instrumental effects are not – or only partly included.

We use the following H_2O line and continuum and dry air models for the calculations presented in this paper.

Frequency range 1 – 1000 GHz

The absorption due to water vapor is modeled as described in Pardo et al. [2001]: all H_2O lines up to 10 THz are calculated in order to account for the H_2O far-wing absorption below 2 THz. In addition, a pseudocontinuum water vapor absorption ($\propto \nu^2$) is derived from Fourier Transform Spectrometer (FTS) obervations in the 0.5–1.6 THz regime [Pardo et al., 2005]. The absorption due to dry air continua is (i) collisionally induced absorption (N_2 and O_2) that is also contained in the observationally based model of Pardo et al. [2001], and (ii) relaxation (Debye) absorption of O_2 that is implemented using the formalism described in Rosenkranz [1993] and Pardo et al. [2001].

Frequency range 1000 – 2000 GHz

Based on FTS measurements in the 0.5–1.6 THz range, Pardo et al. [2005] showed that the $\propto \nu^2$ approximation for the H_2O pseudocontinuum starts to fail for frequencies >1 THz and that the exponent seems to be lower than 2 for ν >1.1 THz. We thus use the semi-empirical MT-CKD-2004 model (http://www.rtweb.aer.com, Clough et al. [2005]), a continuation of the older CKD-model [Clough et al., 1989]. It includes continuum absorption due to water vapor, nitrogen, oxygen, and CO_2. A new feature is that the self- and foreign continuum models are each based on the contributions from a collision induced component and a line shape component. These are applied to all water vapor lines from the millimetre regime to the visible, and the results are summed to obtain self and foreign continuum coefficients from 0–20000 cm^{-1} (0–600 THz). The high-frequency collision-induced spectrum of nitrogen is extracted from the

formulation of Borysow and Frommhold [1986]. The model is scaled with a factor 1.34 as suggested by Boissoles et al. [2003].

4.3. *Contribution of dry and wet component*

In order to to characterize the different contributions of the transmission, we separated the dry and wet component and performed model calculations for three different altitudes (0, 3000 and 6000m). We used a standard 45° N H_2O-profile (scaled depending on altitude for the wet component to give an integrated column of 0.3 mm of pwv for all altitudes) and a 45° N temperature and pressure profile. Figure 2a shows the purely dry air continuum (Pardo-2001 collisional dry air (N_2-O_2) and O_2-Debye continua) alone and curves including all non-water lines. (For simplification, we did not separate the different continua depending on frequency as explained in Sec. 4.2.) Strong lines from O_2 or O_3 cause significant broad-band absorption, in particular at lower frequencies. The dry air continuum (without O_2 and O_3 lines) is dominated by N_2+O_2 non-resonant absorption below 300 GHz and only by N_2 non-resonant absorption above 300 GHz.

Figure 2b displays the wet component alone (Pardo-2001 H_2O-continuum and all water lines) at a pwv of 0.3mm. The water vapor spectrum is characterized by strong and broad water absorption lines and an increasing continuum absorption with frequency. Though this plot shows only the wet component at 0.3 mm (which is a rather low value, found only at the driest sites on Earth), it is obvious that the absorption due to the wet component – in particular H_2O line absorption – is generally more important than the dry component (lines+continuum). Suitability of a given site for astronomical or atmospheric observations depends largely on the specific (local) weather conditions at the site, including humidity and cloudiness. Here we can only generally state that low humidity and high altitude are both beneficial for the observation conditions, whilst in practise also logistical issues such as accessibility are of major relevance.

4.4. *Assumptions of the model and real atmosphere*

Our model calculations are based on the clear sky assumption, i.e do not include the effect of water clouds and cirrus. Absorption of thin and sub-visual cirrus is typically negligible to radio observations, but the observer should watch out for significant ice and more importantly liquid water clouds which affect the observations or calibration procedures.

Another aspect to consider is the timescale for the stability of the transmission. Even under 'clear-sky' conditions, a variation of the attenuation of the atmosphere due to changes of humidity and temperature causes slow changes in transmission (timescale of several hours) and thus creates difficulties in calibration. This can be corrected for by regularly performing sky-dips. Moving inhomogeneities of the water vapor distribution, however, cause rapid fluctuations (seconds to minutes) in the atmospheric radiation, leading to noise in the observations (called 'seeing' in the optical wavelength range and 'sky noise' in the (sub)mm-range) which are not easy to correct for.

4.5. *Specific input parameters*

Since tropospheric water is the main atmospheric absorber at (sub)-mm wavelengths and varies significantly with time, we need to provide a common base for inter-comparison with results from other models. We thus present model calculations for different amounts of precipitable water vapor (pwv). Taking into account the altitude of the site, we produced different H_2O vertical profiles by scaling the tropospheric part of the U.S. standard profile accordingly (i.e. so that the integrated H_2O column above the site corresponds to a certain pwv).

For O_2 and O_3, H_2O, and the minor species (e.g. NO, N_2O, CO, SO_2, HNO_3, etc.) we use typical mid-latitude vertical profiles. The full set of profiles as well as Temperature (T) and pressure (p) profiles can be found on our website. The T,p-profiles used here are climatological monthly averages (July for ALMA and DOME-C, January for KOSMA and JCMT/CSO) and zonal means over 10 degrees. For example, the site of ALMA at 23°S was obtained by averaging T,p-profiles between 20 and 30 degrees South.

All models shown in this paper were calculated for 90° elevation, i.e. zenith view, and have a frequency resolution of 200 MHz. A large number of additional computations at higher spectral resolution, different water vapor columns as well as zooms into particular frequency ranges of potential interest can be found on our website. There, we also provide graphical displays and numerical data files (2-column ascii-format with frequency and transmis-

sion) for more cases, e.g., other Antarctic stations, CCAT, the NASA/DLR aircraft SOFIA (Stratospheric Observatory for Infrared Astronomy), and balloon experiments.

4.6. *Transmission for selected sites*

Figures 3 to 7 show the results of our forward calculations in the frequency range 0–2000 GHz (frequency resolution 200 MHz) for four different observatories. We selected the KOSMA (Gornergrat, Swiss Alps) and CSO/JCMT (Mauna Kea) sites because atmospheric HCN observations with these telescopes will be presented in Paper-II. The ALMA/APEX (Chajnantor) site is of large importance for astronomy and represents a very high-altitude (∼5000 m) site at a latitude of about 23°S. DOME-C is a potentially very interesting location for performing aeronomy observations related to polar ozone chemistry since it is located inside the Antarctic polar vortex at 75°S,123°W (Concordia station at 3260m altitude, see http://www.concordiastation.org). Calculations were done using three different amounts of precipitable water vapor, depending on site and published literature. We thus chose for KOSMA a pwv of 0.5, 1, and 2mm while Mauna Kea, DOME-C, and ALMA show smaller pwv's on average so that we run models with pwv=0.3, 0.6, and 1mm. We want to emphasize that in this study, we only present transmission curves and do not discuss the general 'quality' of different sites. For that, statistics on the cumulative probability for the fraction of time above a certain transmission value have to be considered as well as other meterological factors like atmospheric stability, wind etc.. See, e.g., Lawrence et al. [2004] and Minier et al. [2009 in prep.] for DOME-C,Marks [2002] for DOME-A, and Oterola et al. [2005] for ALMA.

4.6.1. *KOSMA (3200m)*

It becomes obvious from Fig. 3 – and is known since long – that the millimetre wavelengths range (up to 400 GHz) has the best transmission with values better than 40% even for a pwv of 2mm. However, a few strong and broad absorption lines of H_2O, O_2, and O_3, are present in this frequency range. These are for example O_2 lines at 60 and 119 GHz and the H_2O line at 183 GHz. Since the atmosphere is very transparent in this frequency range for all sites discussed in this paper, we will not go into more details here but focus on the higher frequency ranges (>400 GHz). Only a few atmospheric windows open at ∼410, 480, ∼660, and 850 GHz where a transmission of up to 40% can be reached. The THz-range, however, has only few windows: one at 1050 GHz, one at 1300 GHz, and one at 1500 GHz with a transmission rarely above 10%. Successfull astronomical observations at KOSMA were performed at frequencies of around 115, 230, 345, 461, 492, and 806/809 GHz and thus demonstrate the capability of this site as a sub-mm observatory. Further information on the atmospheric transparency at KOSMA can be found at http://ph1.uni-koeln.de/kosma and in [Kramer and Stutzki, 1990].

4.6.2. *JCMT/CSO (4100m)*

Transmission curves for 0.3, 0.6, and 1mm pwv are displayed in Fig. 4. Although the higher altitude of Mauna Kea compared to the KOSMA site in the Swiss Alps increases the transparency of the atmosphere, this effect is only significant at high frequencies. The windows at 660 and 850 GHz have a transmission of 30% for pwv=1mm at Mauna Kea while at KOSMA, the transmission at the same pwv is 5% less. In contrast to KOSMA, the high-frequency windows now open up with transmissions up to 20% and thus allow occasionally observations of atmospheric tracers as well as astronomically interesting lines up to 950 GHz (e.g., NH_2 at 902 GHz). Experimental observations above 1 THz become feasible (e.g., NH^+ at 1.0126 THz, p-H_2D^+ at 1.37 THz, [NII] at 1.46 GHz. Observable lines for aeronomy are for example CO, NO, NO_2, OH, HO_2, H_2CO, HOCl, HOBr, HCN. Some other trace gases like N_2O, OCS, and CH_3Cl have their maximum emission below 1 THz. The reason for the better transmission is the higher altitude of the site (3200m for KOSMA and 4100m for Mauna Kea) and the generally (slightly) lower pwv. A comparison with a transmission calculator (see http://www.submm.caltech.edu/cso/weather/atplot.shtml) provided on the CSO website (based on the ATM model of Pardo et al. [2001]) shows a deviation to ATM of less than 5% for all frequency ranges and values of pwvs. This is an interesting result, in view of the different implementations of the two programs and different input values for water, temperature, and pressure profiles. Intercomparison of clear-sky radiative transfer models [Melsheimer et al., 2005], when the user had the free choice of selecting spectroscopic data and con-

tinuum model for their calculation, show difference of 10% at mm wavelength.

One advantage of the Mauna Kea site is that the water line at 183 GHz [Wiedner et al., 2001], and the continuum opacity at 225 GHz are continuosly monitored with dedicated radiometers. This allows a precise calibration of data and to establish a helpful statistics on the diurnal and yearly variation of the optical depth at 225 GHz (τ_{225}). It was found that τ_{225} and the precipitable water are related by $\tau_{225} = 0.01 + 0.04\,\mathrm{pwv}$ and that the opacity at higher frequencies, i.e. 345 GHz, can be calculated by $\tau_{345} = 0.05 + 2.5\,\tau_{225}$. The opacity at any frequency up to 1.6 THz can be accurately calculated using the WVM measurements at 183 GHz [Pardo et al., 2004].

4.6.3. *ALMA (5100m)*

As stated on the website of the APEX radiotelescope (http://www.apex-telescope.org/sites/chajnantor/atmosphere), the median pwv is 1mm but can occasionally fall below 0.3mm. Conditions of pwv<0.5mm can be expected up to 25% of the time between April and December (the interval between December and April is used for technical work and commissioning of new instruments and could potentially be considered for long-term atmospheric monitoring projects). We thus run models for pwvs of 0.3, 0.6, and 1mm and display the results in Fig. 5. The absoute difference of transmission compared to the Mauna Kea site is typically smaller than 10% over all frequency ranges. What makes ALMA an exceptional site is the high cumulative probablity of pwv values below 1mm [Otorola et al., 2005].

A first order comparison with the ATM model in the frequency range 10 to 1610 GHz (that is provided by a web-based calculator, see http://www.apex-telescope.org/sites/chajnantor/atmosphere/atm.pwv/) for the same pwv's values shows a typical deviation of 5-10% between the results. In general, the ATM model is more optimistic than MOLIERE-5, but the general agreement is very good. Since the comparison ATM/MOLIERE-5 for the CSO website was even better (deviations of less than 5%) it has to be clarified why the difference for the ALMA site is larger. This is either due to the temperature, pressure, and H_2O profiles and/or different versions of the ATM model for Mauna Kea and ALMA site.

4.6.4. *DOME-C (3200m)*

The transmission curves for the DOME-C site (Fig. 6) for values of pwv=0.3, 0.6, and 1mm are typically 5–10% lower than the ones for ALMA. Below 1 THz, the difference is 10% and above 1 THz the difference becomes smaller with a transmission of up to 15% for the high-frequency windows for ALMA and 10% for DOME-C.

Site-testing studies for DOME-C (see e.g. [Minier et al., 2008] for a summary) show that the absolute values for pwv can drop very low. We thus run models of pwvs of 0.1, 0.2, and 0.3 mm, shown in Fig. 7. For exceptional conditions, i.e. pwv around 0.1mm, the transmission in some THz-windows of interest can go up to 30%. This is, however, also true for the ALMA site (5100m) and possible future sites like that chosen for CCAT (5600m) or DOME-A (4100m). In fact, CCAT – due to its higher altitude – offers an even better transmission at the same pwv than all other sites investigated in this study (see webpage for more info). Recent, long-term measurements at 200 μm [Tremblin et al. 2009, in prep.] show, however, that Dome C is a better site than the best Chajnantor site (i.e. mountains at >5500 m) in terms of pwv percentiles.

To explore in more detail the quality of the DOME-C site in the mid-IR wavelength range, we run a model at pwv=0.2mm for frequencies up to 10 THz (∼3mm to 30 μm). Figure 8 demonstrates that several windows open between 30 and 50 μm. Astronomical continuum observations in this wavelength range trace, for example, warm dust in star forming regions. Combined with continuum data in the FIR range (in the 200, 350, 450, and 870 μm windows), this will allow to derive spectral energy distributions and thus the temperature of astrophysical objects. Several bolometers are already available for these wavelengths ranges: SHARC-II [Dowell et al., 2001] at 350μm installed at the CSO, LABOCA (http://www.mpifr-bonn.mpg.de/div/bolometer) at 870 μm at APEX, and p-ARTEMIS [Talvard et al., 2006] at 450 μm [André et al., 2008] at APEX (200 and 350 μm are planned for a future ARTEMIS instrument).

5. Summary

We compiled basic properties and technical characteristics (optics, front- and back-ends, observ-

ing modes, calibration) of radiotelescopes with regard to their use for atmospheric line observations. Extensive tables inform about telescope's location, instrumentation and technical details as well as a web site for further information (http://transmissioncurves.free.fr). We conclude that many radiotelescopes offer a good potential to be used for atmospheric line observations and encourage the aeronomy community to consider this potential.

The capacity of the MOLIERE-5 radiative transfer model was demonstrated to produce transmission spectra for four astronomical observatory sites (KOSMA, Mauna Kea, ALMA, DOME-C) for frequencies between 0 and 2 THz (up to 10 THz for DOME-C). These transmission curves are very useful to deduce the quality of a site for astronomical or atmospheric observations in the millimeter to FIR range. Results of model runs for other sites in form of graphical displays and ascii-data are given on a dedicated website.

Acknowlegement We thank F. Boes for providing us with figures, and C. Kramer and V. Minier for providing information concerning high-frequency spectral lines and DOME-C site testing. We also thank D. Despois for useful discussions on HCN and radiotelescopes.

References

Allan, D., June 1972. Statistics of atomic frequency standards, precision measurement and calibration: selected nbs papers on frequency and time. Edition. Vol. 5 of NBS Special Publication 300. US Goverment Printing Office - Washington, DC, pp. 466–, edited by B.E. Blair and A.H. Morgan.

André, P., Minier, V., Gallais, P., et al., 2008. First 450 μm dust continuum mapping of the massive star-forming region NGC3576 with the P-ArTéMiS bolometer array. Astronomy & Astrophysics 490, L27.

Barret, A., Chung, V., 1962. A method for the determination of high altitude water vapour abundance from ground-based mm-observations. J. Geophys. Res. 67, 4295–4266.

Bevilaqua, R., Olivero, J., Schwartz, P., 1983. An observational study of water vapour using ground-based microwave techniques. J. Geophys. Res. 88, 8523–.

Boes, F., 1994. Kohlenstoffmonoxid in der Mesosphäre. Ph.D. thesis, University of Cologne.

Boissoles, J., Boulet, C., Tipping, R., Brown, A., Ma, Q., 2003. Theoretical calculation of the translation-rotation collision-induced absorption in N_2-N_2, O_2-O_2 and N_2-O_2 pairs. Jour.of Quant.Spec. & Radiative Transfer 1-4, 505–.

Borysow, A., Frommhold, L., December 15 1986. Collision-induced rototranslational absorption spectra of N_2-N_2 pairs for temperatures from 50 to 300 K. Astrophysical Journal 311, 1043–1057.

Burrows, S., Martin, C., Roberts, E., 2007. High-latitude remote sensing of mesospheric wind speeds and carbon monoxide. J. Geophys. Res. 112, 134–.

Calisesi, Y., Wernli, H., Kämpfer, N., 2001. Mid-stratospheric ozone variability over Bern related to planetary wave activity during the winters 1994-1995 to 1998-1999. J. Geophys. Res. 106, 7903–7916.

Caton, W., Manella, G., Kalgahan, P., 1968. Radio measurements of the atmospheric ozone transition. Astrophysical Journal 151, L153–L156.

Clough, S., Kneizys, F., Davies, R., 1989. Line shape and the water vapor continuum. Atmos. Res. 23, 229–241.

Clough, S., Shepard, M., et al., E. M., 2005. Atmospheric radiative transfer modeling. Journal of Quant. Spec. and Rad. Transfer 91, 233.

Table 1
Sites of (sub)millimeter-wave radiotelescopes.

Site	⌀ [m]	Location	Geographical Longitude/Latitude	Altitude [m]	Website http://
CfA[a]	1.2	Cambridge/USA	∼74°00′W, 40°42′N	6	cfa-www.harvard.edu/cfa/mmw
KOSMA[b]	3	Gornergrat/Switzerland	7°47′42″E, 45°59′2″N	3200	www.ph1.uni-koeln.de/kosma
NANTEN2	4	Pampa la Bola/Chile	∼67°45′E, 23°00′S	4865	www.ph1.uni-koeln.de/nanten2
SRAO	6	Seoul/Korea	∼37°27′15″E, 126°57′19″S	181	srao.snu.ac.kr
SMT[c]	10	Mt. Graham/USA	109°53′28.5″W, 32°42′5.8″N	3186	aro.as.arizona.edu
ASTE[d]	10	Pampa La Bola/Chile	67°42′11″W,22°58′18″S	4860	www.nro.nao.ac.jp/ aste
CSO[e]	10	Mauna Kea/Hawaii	155°28′47″W, 19°49′33″N	4092	www.submm.caltech.edu/cso
APEX[f]	12	Chajnantor/Chile	67°42′11″W, 23°00′20.8″S	5105	www.apex-telescope.org
KP12m[g]	12	Kitt Peak/USA	111°36′53.475″W, 31°57′12″N	1914	aro.as.arizona.edu
Qinghai	13.7	Delingha/China	97°33′36″E, 37°22′24″N	3200	www.pmodlh.ac.cn/13.7m_telescope
Metsähovi	14	Kylmälä/Finland	24°23′35″E, 60°13′4″N	60	kurp-www.hut.fi
JCMT[h]	15	Mauna Kea/Hawaii	155°28′47″W, 19°49′33″N	4092	www.jach.hawaii.edu/JCMT
OSO[i]	20	Onsala/Sweden	11°55′34.9″E, 57°23′45″N	23	www.chalmers.se/rss/oso-en
Mopra	22	Coonabarabran/Australia	31°16′04″E, 149°05′58″S	866	www.narrabri.atnf.csiro.au
IRAM[j]	30	Sierra Nevada/Spain	3°23′33.7″W, 37°3′58.3″N	2920	iram.fr
NRO[k]	45	Nobeyama/Japan	142°43′2″, 35°56′29.5″N	1350	www.nro.nao.ac.jp

[a]Center for Astrophysics, [b]Kölner Observatorium für Sub-Mm Astronomie, [c]SubMillimeter Telescope, [d]Atacama Submillimeter Telescope Experiment, [e]Caltech Submillimeter Observatory, [f]Atacama Pathfinder EXperiment, [g]Kitt Peak 12 meter Telescope, [h]James Clark Maxwell Telescope, [i]Onsala Space Observatory, [j]Institut Radio Astronomie Millimetrique, [k]Nobeyama Radio Observatory.

Connor, B., Barrett, J., Parrish, A., 1987. Ozone over McMurdo Station. J. Geophys. Res. 92, 13221–.

Crewell, S., Cheng, D., de Zafra, R., Trimble, C., 1995. Millimeter wave spectroscopic measurements over the south pole, I: A study of stratospheric dynamics using N_2O observations. J. Geophys. Res. 100, 20839–20844.

de Zafra, R., Smyshlyaev, S., 16 October 2001. On the formation of HNO_3 in the Antarctic mid to upper stratosphere in winter. J. Geophys. Res. 106 (D19), 23115–23125.

de Zafra, R. L., Muscari, G., March 2004. CO as an important high-altitude tracer of dynamics in the polar stratosphere and mesosphere. J. Geophys. Res. 109 (D18), 6105–+.

Despois, D., Ricaud, P., Lautié, N., Schneider, N., Jaqc, T., Biver, N., Lis, D., Chamberlin, R., Phillips, T., Miller, M., Jenniskens, P., 2000. Search for extraterrestrial origin of atmospheric trace molecules - Radio sub-mm observations during the Leonids. Earth, Moon, and Planets 82-83, 129–140, special issue: Leonid storm.

Dowell, C., Collins, W., Gardner, M., et al., 2001. SHARC II, a Second Generation 350 Micron Camera for the CSO. Bulletin of the American Astronomical Society 33, 792.

Encrenaz, T., Lellouch, E., Atreya, S., Wong, A., 2004. Detectability of minor constituents in the martian atmosphere by IR and submm spectroscopy. Planetary and Space Science 52, 1023–.

Eriksson, P., 1999. Microwave radiometric observations of the middle atmosphere: Simulations and inversions. Ph.D. thesis, Chalmers University of Technology, Göteburg, Sweden, technical report No. 355, School of Electrical and Computer Engineering, ISBN 91-7197-757-0.

Forkman, P., Eriksson, P., Murtagh, D., Espy, P., 2005. Observing the vertical branch of the mesospheric circulation at latitude 60°N using ground-based measurements of CO and H_2O. J. Geophys. Res. 110 (D05107), doi:10.1029/2004JD004916.

Frisk, U., Hagström, M., Ala-Laurinaho, J., et al., May 2003. The Odin satellite: I. Radiometer design and test. Astronomy & Astrophysics 402 (3), L27–34.

Groom, D., 1965. Stratospheric thermal emission and absorption neat the 1.35 cm line of water vapour. J. Atmos. Terr. Phys. 27, 217–233.

Kasai, Y., Takahashi, C., Urban, J., Hoshino, S.,

Takahashi, K., Inatani, J., Shiotani, M., Masuko, H., March 2006. Stratospheric Ozone Isotope Enrichment Studied by Sub-Millimeter Wave Heterodyne Radiometry: The Observation Capabilities of SMILES. IEEE Transactions on Geoscience and Remote Sensing 44 (3), 676–693.

Klein, U., Wohltmann, I., Lindtner, K., Künzi, K., 2002. Ozone depletion and chlorine activation in the Arctic winter 1999/2000 observed in Ny-Alesund. J. Geophys. Res. 107 (D20), 8288–, doi:10.1029/2001JD000543.

Kramer, C., Stutzki, J., 1990. Atmospheric Transparency at Gornergrat, Univ. of Cologne. Technical Mem. 5.

Kraus, J., 1986. Radio Astronomy. Cygnus-Quasar Books. Powell.

Lautié, N., 2003. Traitement des mesures satellitaires sub-millimétriques effectuées par Odin/SMR; étude non-linéaire de la vapeur d'eau. Étude stratosphérique de HCN au moyen de mesures micro-ondes. Ph.D. thesis, Université Paris VI, France.

Lawrence, J., Ashley, M., Tokovinin, A., Travouillon, T., 2004. Exceptional astronomical seeing conditions above DOME-C in Antarctica. Nature 431.

Liebe, H., Hufford, G., Cotton, M., 17-21 May 1993. Propagation modeling of moist air and suspended water/ice particles at frequencies below 1000 GHz, AGARD 52nd Specialists Meeting of the Electromagnetic Wave Propagation Panel, Palma De Mallorca, Spain.

Lobsiger, E., Künzi, K., Dütsch, H., 1984. Comparison of stratosperic ozone profiles retrieved from microwave radiometer and Dobson spectrometer data. J. Atm. and Terr. Phys. 46 (9), 799.

Lord, S., 1992. A new software tool for computing earth's atmospheric transmission of near- and far-infrared radiation. NASA Technical Memorandum (103957).

Marks, R., 2002. Astronomical seeing from the summits of the Antarctic Plateau. Astronomy & Astrophysics 385, 328.

Melsheimer, C., Verdes, C., Buehler, S., et al., 2005. Intercomparison of general purpose clear-sky atmospheric radiative transfer models for the millimeter/sub-millimeter spectral range. Radio Science 40 (RS1007), doi:10.1029/2004RS003110.

Minier, V., Olmi, L., Lagage, P.-O., et al., 2008. Submm/FIR astronomy in Antarctica: Potential for a large telescope facility. In: Science, E. (Ed.), Proc. of the 2nd ARENA Conference, Potsdam, Vol 512.

Muscari, G., Santee, M., de Zafra, R., 2002. Intercomparison of stratospheric HNO_3 measurements over Antarctica: Ground-based millimeter-wave versus UARS/MLS Version 5 retrievals. J. Geophys. Res. 107 (D24), 4809–.

Nedoluha, G., Bevilacqua, R., Gomez, R., Hicks, B., Russell III, J., Connor, B., 10 July 2003. An evaluation of trends in middle atmospheric water vapor as measured by HALOE, WVMS, and POAM. J. Geophys. Res. 108 (D13), 4391, doi:10.1029/2002JD003332.

Oterola, A., Holdaway, M., Nyman, L.-E., Radford, S., Butler, B., 2005. Atmospheric Transparance at Chanjanantor: 1973-2003. ALMA mem. Series 512.

Paine, S., 2004. The AM atmospheric model. SMA Technical Memorandum (152).

Pardo, J., Cernicharo, J., Serabyn, E., 2001. Atmospheric transmission at microwaves (atm): an improved model for mm/submm applications. IEEE Transactions on Antennas and Propagation 49 (12), 1683–.

Pardo, J., Pagani, L., Gérin, M., Prigent, C., 1995. Evidence of Zeeman splitting in the 21-01 rotational transition of atmosp. $^{16}O^{18}O$. J. Quant. Spectrosc. Radiat. Transfer 54 (6), 931–.

Pardo, J., Serabyn, E., Wiedner, M., Cernicharo, J., 2005. Measured telluric continuum-like opacity beyond 1 THz. Jour. of Quant. Spec.& Rad. Transfer 96, 537–.

Pardo, J., Wiedner, M., Serabyn, E., et al., 2004. Side-by-side comparison of fts and wvr as tools for the calibration of mm/submm ground-based observatories. Astrophysical Journal Supplement 153, 363.

Parrish, A., de Zafra, R., Solomon, P., 1981. ClO in the stratospheric ozone layer: Ground-based detection and measurement. Science 211, 1158–.

Parrish, A., de Zafra, R., Solomon, P., Barrett, J., 1988. A ground based technique for millimeter wave measurements of stratospheric trace constituents. Radio Science 23 (2), 106–118.

Penzias, A., Burrus, C., 1973. Millimeter-Wavelength Radio-Astronomy Techniques. Annual Review of Astronomy and Astrophysics 11, 51–.

Pickett, H., Poynter, R., Cohen, E., Delitsky, M., Pearson, J., Müller, H., 1998. Submillimeter, millimeter, and microwave spectral line catalog. J. Quant. Spectrosc. Radiat. Transfer 60 (5), 883–890.

Prigent, C., Pardo, J., Rossow, W., 2006. Comparisons of the mm and submm bands for atmospheric temperature and water vapor soundings from clear and cloudy skies. Journal of Applied Meteorology and climatology 45, 1622–.

Raffalski, U., Hochschild, G., Kopp, G., Urban, J., 2005. Evolution of stratospheric ozone during winter 2002/2003 as observed by a ground-based millimetre wave radiometer at Kiruna, Sweden. Atmospheric Chemistry & Physics 5, 1–9.

Ricaud, P., Baron, P., de La Noë, J., 2004. Quality assessment of ground-based microwave measurements of ClO, O_3, NO_2 from the NDSC radiometer at the Plateau de Bure. Annales Geophysicae 22, 1903–1915.

Ricaud, P., Brillet, J., de La Noë, J., Parisot, J., 1991. Diurnal and seasonal variations of stratomesopheric ozone. J. Geophys. Res. 96, 18617–.

Rosenkranz, P., 1993. Absorption of Microwaves by Atmospheric Gases, Atmospheric Remote Sensing by Microwave Radiometry Edition. Wiley Series in Remote Sensing. M.A. Janssen, New York, Ch. 2, pp. 37–82, ISBN 0-471-62891-3.

Rothman, L., Rinsland, C., Goldman, A., et al., November 1998. The HITRAN Molecular Spectroscopic Database and HAWKS (HITRAN Atmospheric Workstation): 1996 Edition. J. Quant. Spectrosc. Radiat. Transfer 60, 665–710.

Sandor, B., Clancy, R., 1998. Mesospheric HO_2 chemistry. J. Geophys. Res. 103.

Schneider, N., Lezeaux, O., de La Noë, J., Urban, J., Ricaud, P., 2003. Validation of ground-based strato-mesospheric ozone observations. J. Geophys. Res. 108 (D17), 4540+.

Seele, C., Hartogh, P., June 1999. Water vapor of the polar middle atmosphere: Annual variation and summer mesosphere conditions as observed by ground-based microwave spectroscopy. Geophys. Res. Lett. 26, 1517–1520.

Shindell, D. T., de Zafra, R. L., 1996. Chlorine monoxide in the Antarctic spring vortex 2. A comparison of measured and modeled diurnal cycling over McMurdo Station, 1993. J. Geophys. Res. 101, 1475–1488.

Sinnhuber, B.-M., Langer, J., Klein, U., Raffalski, U., Künzi, K., Schrems, O., 1998. Ground based millimeter-wave observations of Arctic ozone depletion during winter and spring 1996/97. Geophys. Res. Lett. 25 (17), 3327–3330.

Solomon, P., de Zafra, R., Parrish, A., 1984. Diurnal variations of stratospheric ClO. Science 224, 1210–.

Steinbrecht, W., Claude, H., Schönenborn, F., McDermid, I. S., Leblanc, T., Godin, S., Song, T., Swart, D. P. J., Meijer, Y. J., Bodeker, G. E., Connor, B. J., Kämpfer, N., Hocke, K., Calisesi, Y., Schneider, N., de La Noë, J., Parrish, A. D., Boyd, I. S., Brühl, C., Steil, B., Giorgetta, M. A., Manzini, E., Thomason, L. W., Zawodny, J. M., McCormick, M. P., Russell, J. M., Bhartia, P. K., Stolarski, R. S., Hollandsworth-Frith, S. M., 2006. Long-term evolution of upper stratospheric ozone at selected stations of the Network for the Detection of Stratospheric Change (NDSC). J. Geophys. Res. 111 (D10308), 10308–.

Talvard, M., André, P., Rodriguez, L., et al., 2006. ARTEMIS: filled bolometer arrays for next generation telescopes. SPIE 6275.

Urban, J., Baron, P., Lautié, N., Dassas, K., Schneider, N., Ricaud, P., de La Noë, J., 2004a. MOLIERE (v5): A versatile forward- and inversion model for the millimeter and sub-millimeter wavelength range. J. Quant. Spectrosc. Radiat. Transfer 83 (3-4), 529–554.

Urban, J., Dassas, K., Ricaud, P., Forget, F., April 2005a. Retrieval of vertical constituents and temperature profiles from passive sub-millimeter wave limb observations of the Martian atmosphere: a feasibility study. Applied Optics 44, 2438–2455.

Urban, J., Küllmann, K., Künzi, K., Wohlgemuth, J., Goede, A., Kleipool, Q., Whyborn, N., Schwaab, G., Chipperfield, M., 2000a. Stratospheric ClO across the edge of the of the Arctic polar vortex: Measurements of the Airborne--Submillimeter-SIS-Radiometer compared to 3-D model calculations. In: Zerefos, C. (Ed.), Chemistry and Radiation Changes in the Ozone layer. Vol. 557 of Nato Science Series C. Kluwer Academic Publishers, pp. 233–240, ISBN 0-7923-6513-5.

Urban, J., Lautié, N., Le Flochmoën, E., Jiménez, C., Eriksson, P., Dupuy, E., El Amraoui, L., Ekström, M., Frisk, U., Murtagh, D., de La Noë, J., Olberg, M., Ricaud, P., July 2005b. Odin/smr limb observations of stratospheric trace gases: Level 2 processing of clo, n_2o, o_3, and hno_3. J. Geophys. Res. 110, D14307.

Urban, J., Lautié, N., Murtagh, D., Eriksson, P., Kasai, Y., Loßow, S., Dupuy, E., de La Noë, J., Frisk, U., Olberg, M., Le Flochmoën, E., Ricaud, P., June 2007a. Global observations of middle atmospheric water vapour by the Odin satellite: An overview. Planetary and Space Science 55 (9),

1093–1102, special issue 2nd General Assembly of Asia Oceania Geophysical Society (2005): Highlights in Planetary Science.

Waters, J., Froidevaux, L., Harwood, R., et al., 2006. The Earth observing system microwave limb sounder on the Aura satellite. IEEE Trans. Geosci. Remote Sensing 44 (5).

Waters, J., Wilson, T., Shimabukuro, F., 1976. Microwave measurements of mesospheric CO. Science 192, 1174.

Wieching, G., 2007. CONDOR: a Heterodyne Receiver for Astronomical Observations at 1.5 THz. PhD Thesis, University of Cologne.

Wiedner, M., Hills, R., Carlstrom, J., et al., 2001. Interferometric Phase Correction using 183 GHz Water Vapor Monitors. Astrophysical Journal 553, 1039.

Wiedner, M., Wieching, G., et al., F. B., 2006. First observations with CONDOR: a 1.5 THz Heterodyne Receiver . Astronomy & Astrophysics 454, L33.

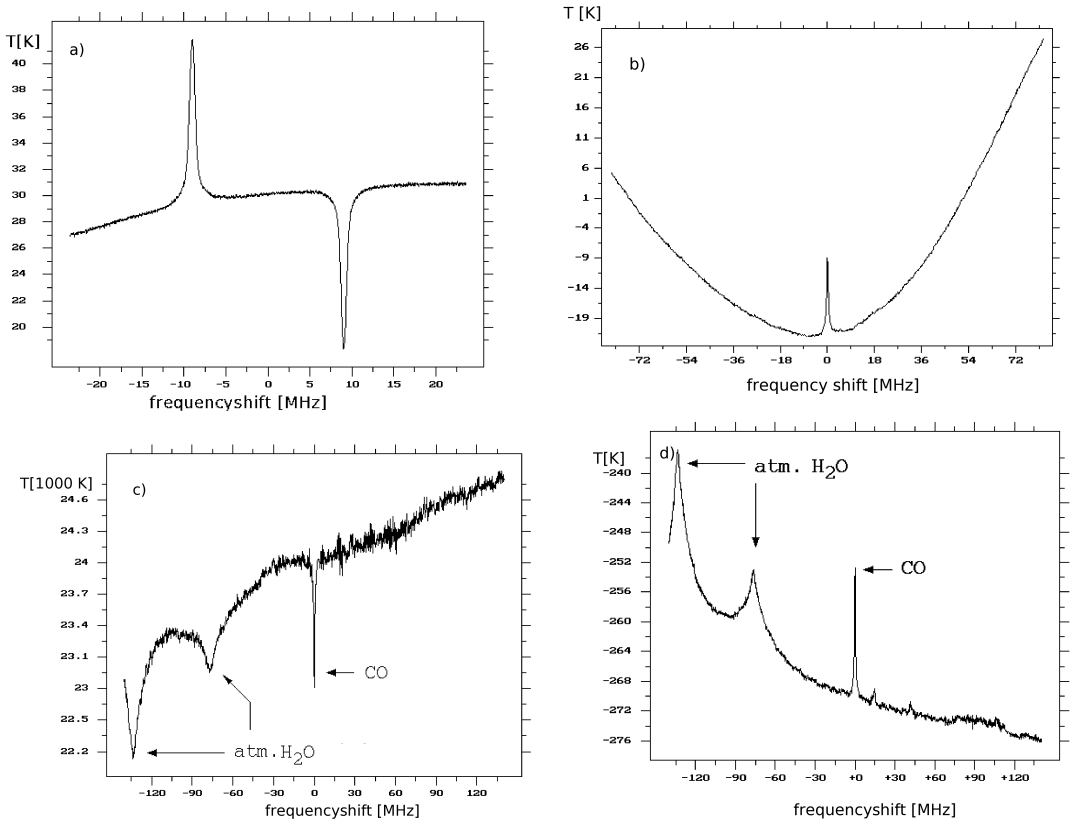

Fig. 1. Examples of mesospheric ^{12}CO 2→1 measurements at 230 GHz, taken with the KOSMA 3m telescope Boes [1994]. All observations were performed with a Schottky receiver (T_{rec} ∼400 K) and an acousto optical spectrometer (AOS) with a bandwidth of 287 MHz and a spectral resolution of 167 kHz. The integration time is typically one hour. a) Simple frequency switching observation, b) load swichting observation using the cold load as reference, c) absorption measurement against the sun, and d) absorption measurement against the mountains.

Table 2
Technical Specifications of Radiotelescopes.

Site	Freq. Range[a] [GHz]	Type/Band[b]	T^c_{rec} [K]	BW^d_{rec} [GHz]	IF[e] [GHz]	Spec.[f]	BW^g_{spec} [MHz]	Spectral res. [kHz]	Obs. Mode[h]	FWHM[i] [″]
CfA	115	SIS/SSB	65	1	1.4	FB	128	250,500	PS,FS	480
KOSMA	210–270	SIS/DSB	150	1	1.4	AOS	60–1000	50–1100	PS,LS,BS,FS	130
	330–365	SIS/DSB	100	1	1.4				PS,LS,BS,FS	80
NANTEN2	455–495	SIS/DSB	150	1	1.5	AOS	4×1000		PS,LS,BS,FS	40
	795–881	SIS/DSB	500–700	1	1.5				PS,LS,BS,FS	22
SRAO	110/230	SIS/SSB	60			AC	50/100	12–50	PS,BS	48
SMT	130–300	SIS/SSB		2	5	AOS	1000	900	PS,BS	58–25
	320–375	SIS/DSB	125	1	1.5	FB	250–2048	385,1000	PS,BS	22
	425–500	SIS/DSB	110–150	0.8	4–6	CTS	215	40	PS,BS	16.5
	652–720	SIS/DSB	70–95						PS,BS	11
ASTE	324–366	SIS/DSB	125	4	4–8	FB	128, 512	125,500		22
						FFTS	4000	2000		
CSO	195–280	SIS/DSB	50	1	1.2–1.8	AOS	50-1500	50–700	PS,BS,FS	33
	280–420	SIS/DSB	50	1	1.2–1.8	FFTS	500-1000		PS,BS,FS	24
	440–520	SIS/DSB	150	1	1.2–1.8				PS,BS,FS	16.5
	600–720	SIS/DSB	150	1	1.2–1.8				PS,BS,FS	14.5
	780–950	SIS/DSB	250	1	1.2–1.8				PS,BS,FS	11.5
APEX	211–275	SIS/SSB	80		4–8	FFTS	1000	>65	PS,FS	30–25
	275–370	SIS/SSB	135		4–8				PS,FS	23–17
	1250–1384	SIS/DSB	200		2–4				PS, FS	5
KP12m	68–90	SIS/SSB	100	1	1.5	FB	3.8–512	30–2000	PS,BS,FS	90–70
	90–116	SIS/SSB	80	1	1.5	AC	75–600	6–3125	PS,BS,FS	70–55
	133–180	SIS/SSB	125	1	1.5				PS,BS,FS	∼45
Qinghai	85–115	SIS/SSB	60			AOS	42–145	75–209	PS	106×70
Metsähovi	80–115	Schottky/DSB	150		1–1.6	AOS	50–1500	50–700	PS,BS,FS	∼45
	84–115	SIS	100		3.7–4.2				PS,BS,FS	∼45
	129–175	SIS	150		3.7–4.1				PS,BS,FS	∼37
	147	SIS	145		3.7–4.2				PS,BS,FS	∼37
	280–420	SIS/DSB	50	1	1.2–1.8				PS,BS,FS	24
JCMT	211–279	SIS/DSB	70	1.8	4	AC	200–1800	30.5–977	PS,BS,FS	20
	325–375	SIS/DSB	150	1.8	4				PS,BS,FS	14
	430–510	SIS/DSB	330	1.6	4				PS,BS,FS	11
	626–710	SIS/DSB	33	1.6	4				PS,BS,FS	8
OSO	18–50	Schottky	30–50			AC	0.05–1280	0.03–800	PS,BS,FS	210–75
	84–116	SIS/SSB	80–130						PS,BS,FS	44–33
MOPRA	30–50	SIS/SSB	30			FB	8000		PS,FS	115–69
	76–117	SIS/SSB	100						PS,FS	45–30
IRAM	80–115	SIS/DSB	60–80	0.5	1.5	FB	10–1000	3–4000	PS,BS,FS	29–22
	130–183	SIS/DSB	70–125	1	4				PS,BS,FS	14–15
	197–266	SIS/DSB	85–160	1	4				PS,BS,FS	13–9
	241–281	SIS/DSB	125–250	1	4				PS,BS,FS	11–9
	210–276	SIS/DSB	110–380	1	4				PS,BS,FS	12–9
NRO	72–115	SIS/DSB	250–900[j]	0.6		AOS	40,250,480	1,37,250	PS,FS	23–15
	82–116	SIS/DSB	400–800[j]	0.6	2–2.6	AC	4–512	4–500		20–14

[a]Tunable frequency range of the receiver. [b]Type of receiver (SIS or Schottky)/Double-Sideband (DSB) or Single-Sideband (SSB) operation. Some of the receivers are of multi-beam type (not explicitly indicated). [c]Receiver noise temperature (without atmosphere). [d]Receiver bandwidth. [e]Intermediate frequency. [f]Spectrometer type AOS: acousto optical spectrometer, FB:filterbank, AC: autocorrelator, FFTS: Fast Fourier Transform Spectrometer. [g]Spectrometer bandwidth. [h]Observing Modes: PS=Position Switch, LS=Load Switch, BS=Beam Switch, FS=Frequency Switch. [i]Beam Full Width Half Maximum for lower and upper frequency limits.

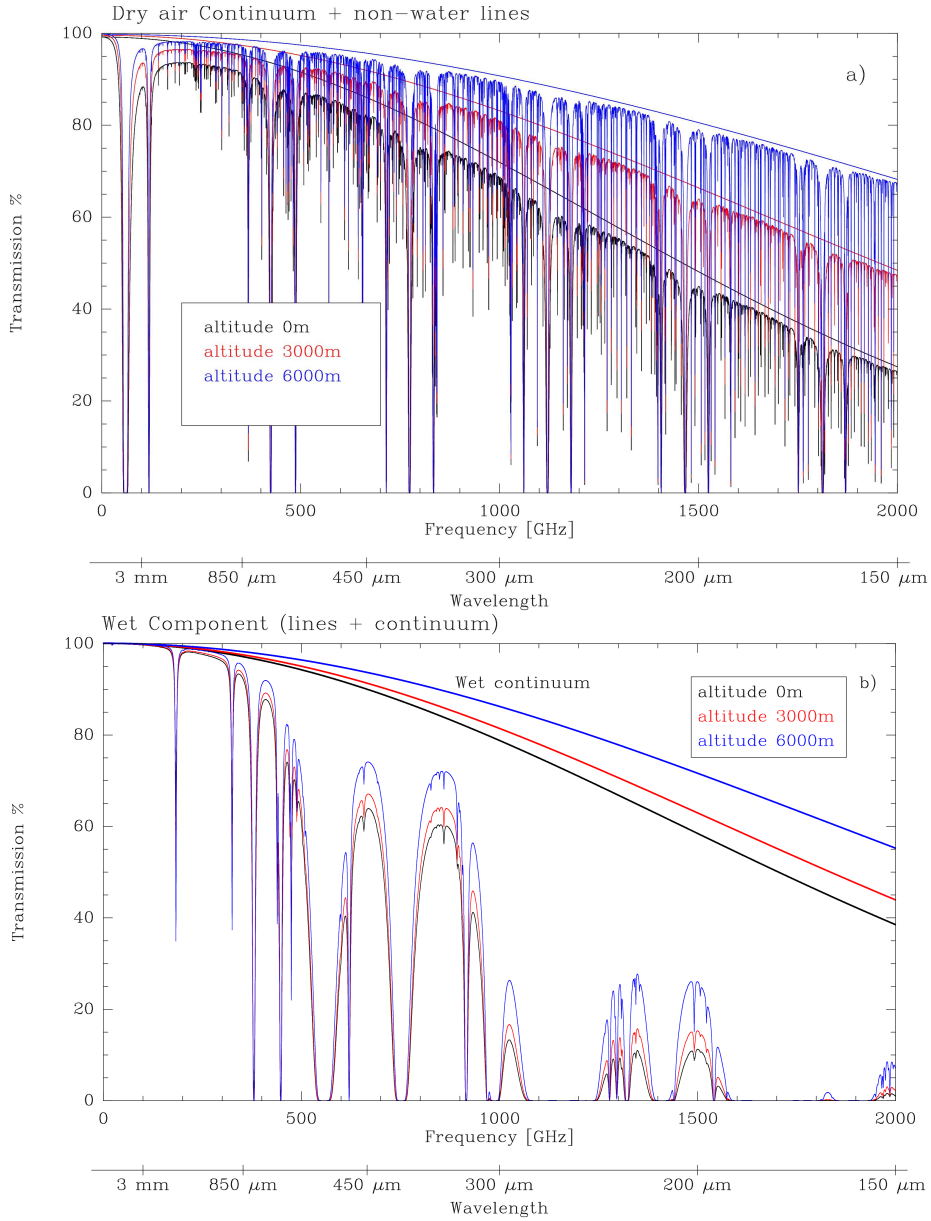

Fig. 2. **a)** Transmission calculated for three different altitudes, considering only the dry air component. The continuous curves show collisionally induced absorption (N_2 and O_2) from the models of Pardo et al. [2001], and relaxation (Debye) absorption of O_2 (Rosenkranz [1993], Pardo et al. [2001]). The other curves contain additional absorption due to all lines except water (including some strong lines like O_2 or O_3). **b)** Transmission calculated for three different altitudes, **only taking into account** the wet component (line and continuum), based on the model of Pardo et al. [2001]. A common pwv of 0.3mm is used. The water continuum alone is included for comparison. The temperature and pressure profiles **for all curves** are from the 45° N U.S. standard atmosphere, the spectral resolution is 400 MHz (dry air) and 200 MHz (wet component), respectively.

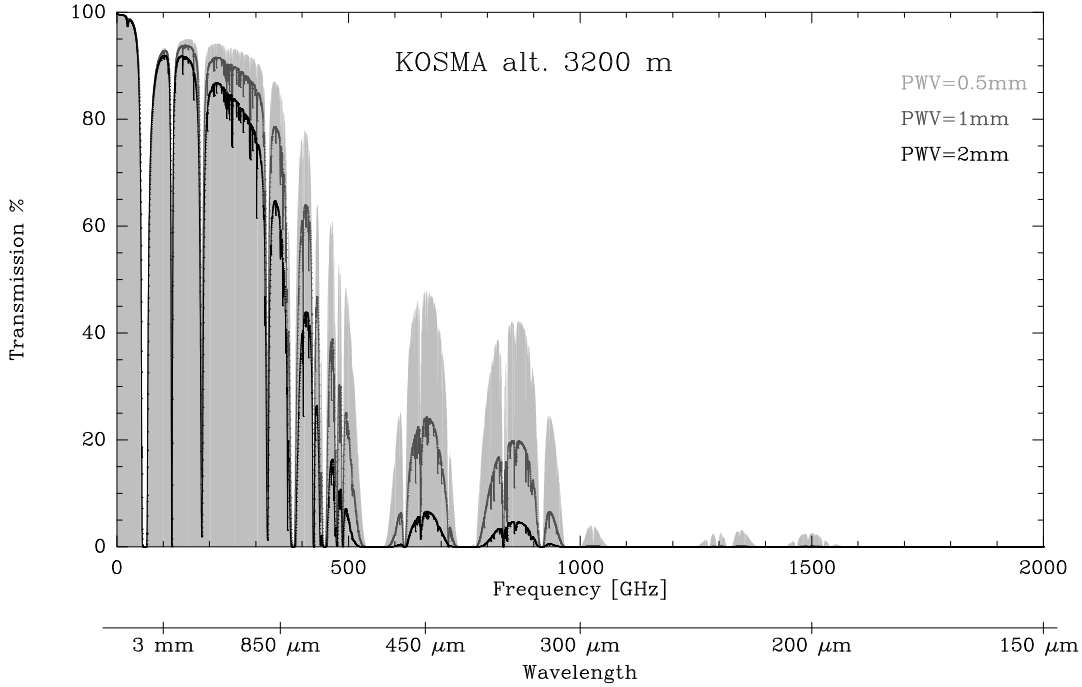

Fig. 3. Transmission curves (in %) for 0.5, 1, and 2 mm precipitable water (pwv) for the KOSMA site (Gornergrat/Switzerland).

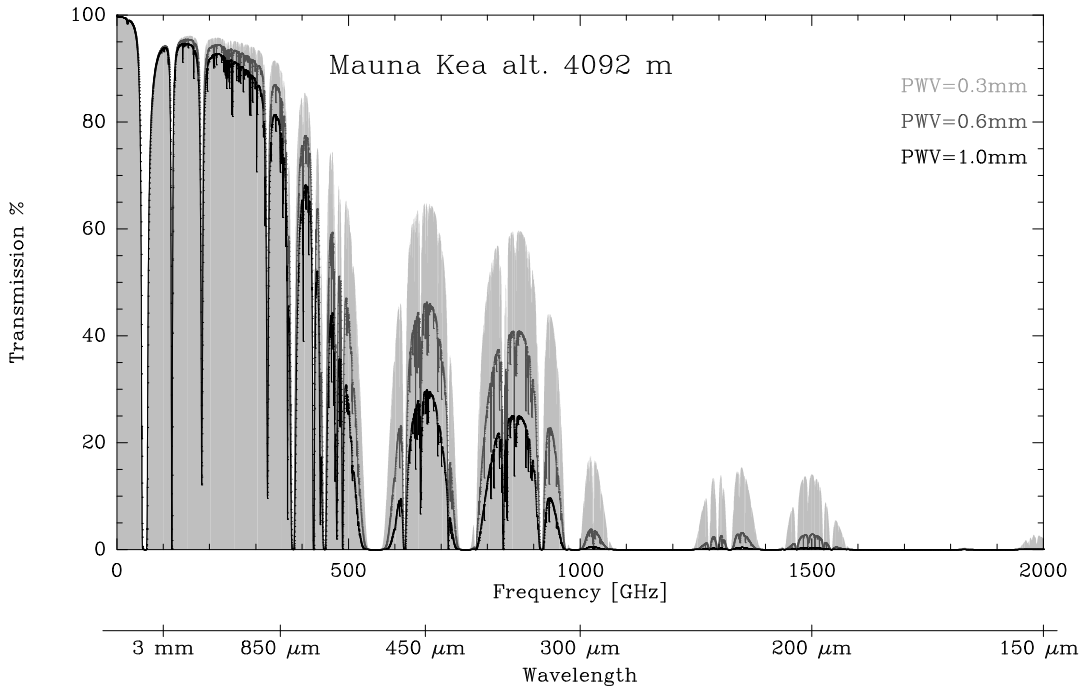

Fig. 4. Transmission curves (in %) for 0.3, 0.6, and 1 mm precipitable water (pwv) for the JCMT/CSO site (Mauna Kea/Hawaii).

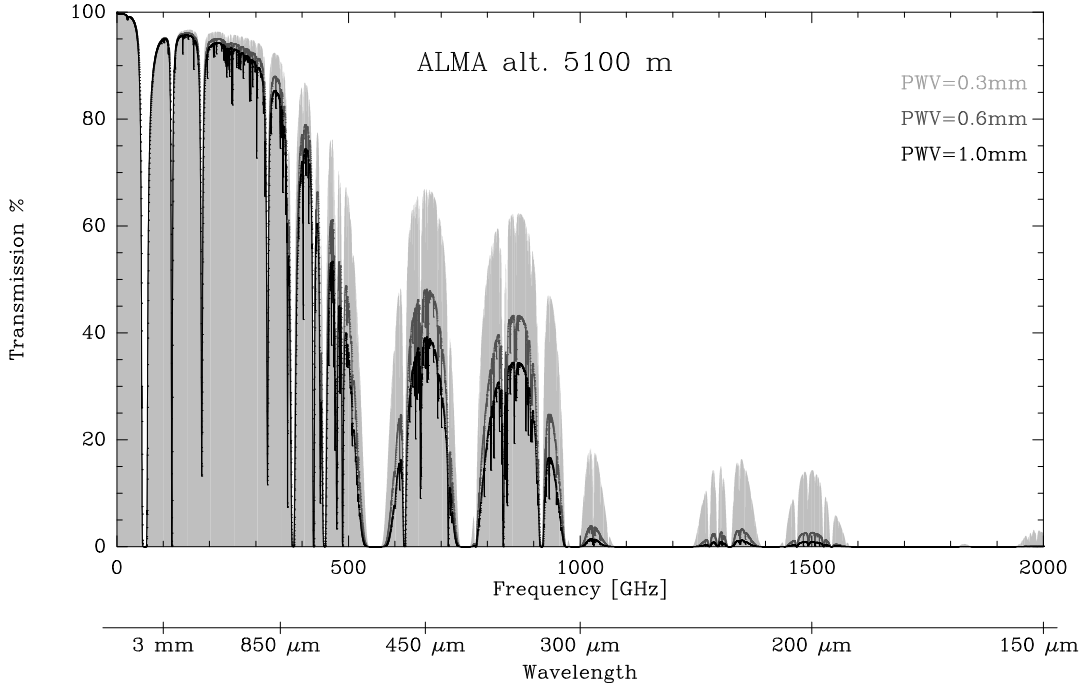

Fig. 5. Atmospheric transmission (in %) for 0.3, 0.6, and 1 mm precipitable water (pwv) for the ALMA/APEX site (Llano de Chajnantor).

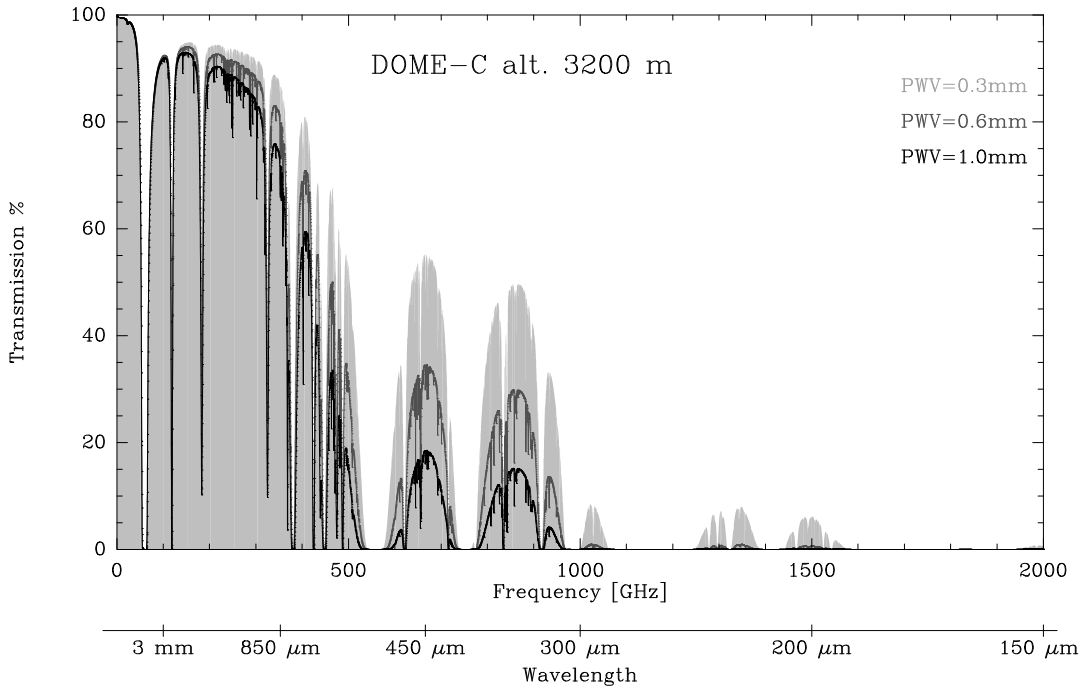

Fig. 6. Atmospheric transmission (in %) for 0.3, 0.6, and 1 mm precipitable water (pwv) for the DOME-C site (Concordia station/Antarctica).

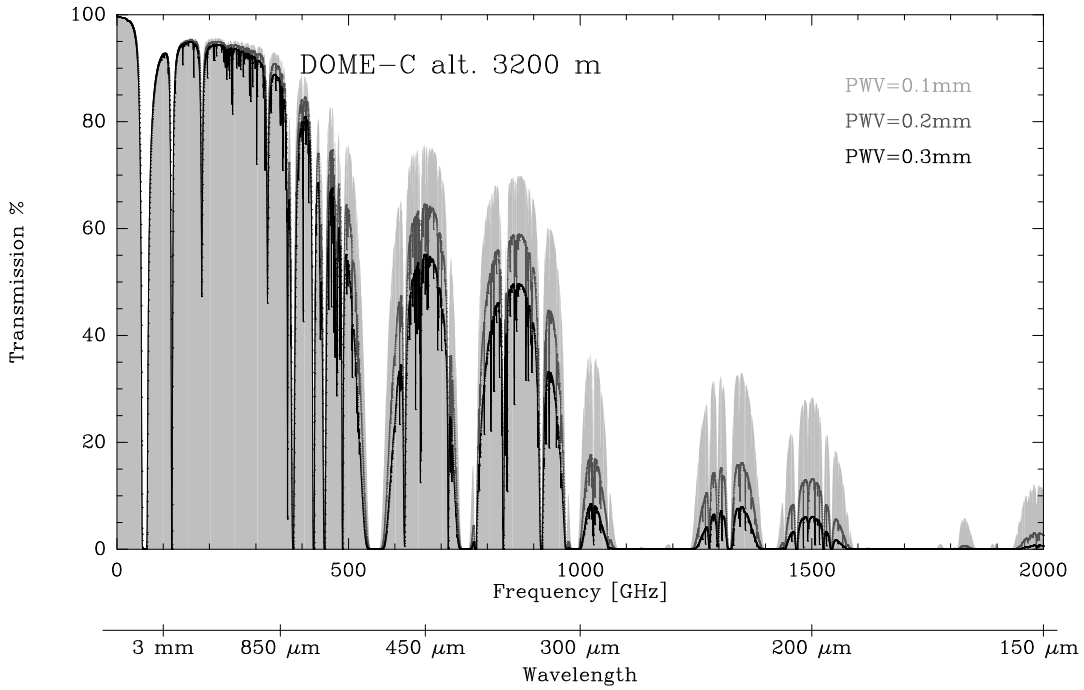

Fig. 7. Atmospheric transmission (in %) for 0.1, 0.2, and 0.3 mm precipitable water (pwv) for the DOME-C site (Concordia station/Antarctica).

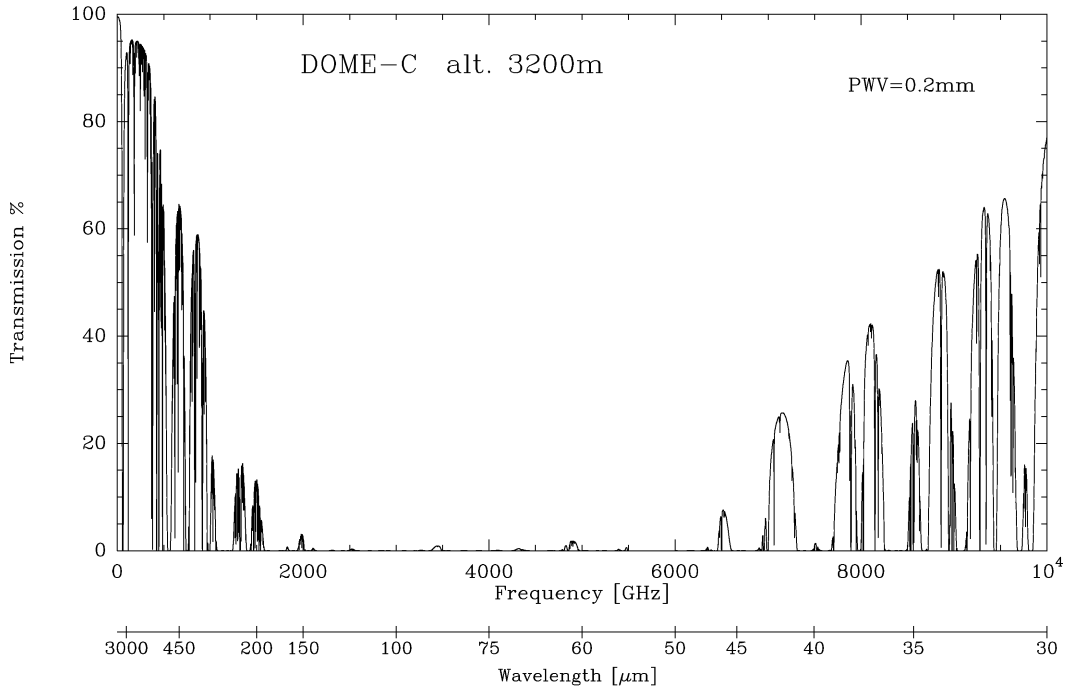

Fig. 8. Atmospheric transmission (in %) for 0.2 mm precipitable water (pwv) for the frequency range 0–10 THz for the DOME-C site (Concordia station/Antarctica). The frequency resolution is 200 MHz. All H_2O and minor species lines up to 10 THz are included.